$La_{0.5}Ce_{0.5}O_{1.75}$-Catalytic Layer for Methane Conversion into C_2 Products Using Solid Oxide Fuel Cell

ECS Transactions, 111 (6) 1957-1964 (2023)
10.1149/11106.1957ecst ©The Electrochemical Society

$La_{0.5}Ce_{0.5}O_{1.75}$-Catalytic Layer for Methane Conversion into C_2 Products Using Solid Oxide Fuel Cell

V. B. Vilela[a], V. V. Thyssen[b], F. F. Fayard[c], L. Massim[d], D. Z. de Florio[e], A. S. Ferlauto[e], M. C. Steil[b], and F. C. Fonseca[a]

[a] Nuclear and Energy Research Institute, IPEN-CNEN, 05508-000, São Paulo, SP, Brazil
[b] Innovation SENAI Institute for Biomass, ISI Biomassa, 79640-250, Três Lagoas, MS, Brazil
[c] Univ. Grenoble Alpes, Univ. Savoie Mont Blanc, CNRS, LEPMI, Grenoble INP (Institute of Engineering and Management), 38000, Grenoble, France
[d] Université de Lyon, Université Claude Bernard Lyon 1, CNRS, IRCELYON, 69626, Villeurbanne Cedex, France
[e] Center for Engineering, Modeling and Applied Social Sciences, Federal University of ABC, 09210-580, Santo André, SP, Brazil

Methane (CH_4), the major constituent of natural gas and biogas, is an abundant source to obtain value-added hydrocarbons. The oxidative coupling of methane (OCM) is a direct catalytic route to convert CH_4 towards C_2 hydrocarbons, ethane (C_2H_6) and ethylene (C_2H_4). Using a solid oxide fuel cell (SOFC) is a strategy to overcome some challenges of fixed-bed catalytic reactors. In this context, we have studied the $La_{0.5}Ce_{0.5}O_{1.75}$ (LCO) oxide as a catalytic layer in a SOFC for methane conversion to C_2. The activity test was carried out at different O^{2-}/CH_4 ratios, varying the anode gas composition, and applied currents.

Introduction

Ethylene (C_2H_4) is a critical building block in the chemical industry with applications in the production of several ubiquitous products such as plastics, solvents, and fertilizers. The primary method of obtaining C_2H_4 is through steam cracking of naphtha from crude oil, an established technology that is difficult to replace. However, the search for sustainable alternatives is ongoing, with natural gas emerging as a viable alternative feedstock. The oxidative coupling of methane (OCM), the primary component of natural gas, offers a direct pathway for converting methane (CH_4) into higher value hydrocarbons, such as C_2 (C_2H_6 and C_2H_4). The rapidly increasing demand for petrochemicals and the abundance of stranded methane reserves are important drivers for more efficient methane conversion routes (1).

Electrochemical technologies, enabled by the increasing availability of green electrons from renewable sources, are gaining value for reactions that are difficult for conventional catalysis. The use of solid-state membrane reactors, such as solid oxide fuel cells (SOFC), to regulate the reactive species and byproducts is a significant development in this field. The electrocatalytic oxidative coupling of methane (EOCM) enables the simultaneous production of C_2 hydrocarbons and electricity when the system operates in fuel cell mode (Equation 1). The operating variables, such as temperature, flow rate, and

CH_4 feed concentration at the anode, and the oxygen supplying by the applied current, are directly related to the correlation between CH_4 conversion and C_2 selectivity (2,3).

$$2CH_4 + 2O^{-2} \leftrightarrows C_2H_4 + 2H_2O + 4e^- \quad [1]$$

To prevent deactivation and allow the application of SOFCs in processes involving substances that contain carbon in its composition, which can form coke and deactivate the cell, strategies have been developed such as the substitution or modification of the Ni/YSZ anode, since Ni does not resist the deposition of coke on the surface of the material (4). The literature reports the use of several ceramic materials (cerium-based, titanates, among others) to replace the Ni-based anode, but these materials showed low electronic conductivity and/or low catalytic activity (5,6).

Pujare and Sammels developed the EOCM in the fuel cell Pt-Sm_2O_3-LSM/YSZ/LSM-Pt and achieved faradaic methane oxidative conversion products C_2H_4, C_2H_6 and C_2H_2 with selectivity of 58 %, 37 %, and 4 %, respectively (7). The benchmark catalyst Mn-Ce-Na_2WO_4/SiO_2 for the OCM fix bed reactor was demonstrated as a catalytic layer in a button SOFC-OCM reactor by Liu's group. The use of this design resulted in a 59.4 % of CH_4 conversion, C_{2+} selectivity of 35.8 % and a C_2H_4/C_2H_6 ratio 2.3 (8). The study developed by Zhu et al. using an $Sr_2Fe_{1.5+x}Mo_{0.5}O_{6-\delta}$-based anode showed a C_2 yield of 16.7 % with 82.2 % C_2 selectivity (9).

The present work aims to study $La_{0.5}Ce_{0.5}O_{1.75}$ prepared by the combustion method, for the application as a catalytic layer at the Ni-YSZ anode of a SOFC for the conversion of methane to C_2 hydrocarbons by the oxidative coupling process.

Experimental

Catalyst Preparation and Characterization

The catalyst $La_{0.5}Ce_{0.5}O_{1.75}$ (LCO) powder was prepared by the combustion method (with excess urea) following the steps described in (10). X-ray diffraction (XRD) analysis of the synthesized catalyst was carried out in the Rigaku MiniFlex II with CuKα radiation, and the crystalline phases were identified by Crystallograhica Search Match© software. Raman spectra were measured using Horiba scientific MacroRaman with a wavelength set at 785 nm. The microstructure of the as-prepared powder was analyzed by a Zeiss Ultra 55 FEG scanning electron microscope (SEM).

To test the OCM properties of the catalyst, a fixed-bed quartz flow reactor was used at atmospheric pressure, with a CH_4:O_2 molar ratio of 4:1 in the reactor feed, 60 mL.min^{-1} of total flow, 20 mg of catalyst, at 800 ºC during 20 h of reaction. An online GC/MSD system was used to analyze the effluent from the reactor. The catalytic activity of the LCO, in both OCM and EOCM, was calculated by Equations 2-6, which represent CH_4 conversion (X_{CH4}), O_2 conversion (X_{O2}), C_2 selectivity (S_{C2}), CO_x selectivity (S_{COx}), and yield (Y_x), respectively.

$$X_{CH4}\ (\%) = 100 \times \text{moles}CH_{4(\text{consumed})} \div \text{moles}CH_{4(\text{feed})} \quad [2]$$

$$X_{O2}\ (\%) = 100 \times moles O_{2(consumed)} \div moles O_{2(feed)} \quad [3]$$

$$S_{C2}\ (\%) = 100 \times (2 \times moles C_{2(formed)}) \div moles CH_{4(consumed)} \quad [4]$$

$$S_{COx}\ (\%) = 100 \times moles CO_{x(formed)} \div moles CH_{4(consumed)} \quad [5]$$

$$Y_X\ (\%) = S_X \times X_{CH4} \quad [6]$$

Preparation of Fuel Cell and EOCM Tests

Electrolyte-supported single cells were prepared using a YSZ-8 (Tosoh) substrate (diameter ~ 19 mm, thickness ~ 0.4 mm). The electrode layers with 1.2 cm^2 of active area, including functional and collector layers, were all deposited by screen-printing (Aurel, C890) on each side of the YSZ electrolyte. The anode was based on NiO/YSZ and calcined at 1400 ºC for 1 h in air. As cathodic materials, $La_{0.65}Sr_{0.30}MnO_3$ (LSM) and LSM/YSZ were used as the current collector and functional cathode layers, respectively. Cathode was sintered at 1100 ºC for 1h in air. A gold wire was attached on the surface of the anode current collector layer with gold paste and annealed at 900 °C in air for 1 h. Then, the LCO catalytic layer was deposited, using the spray-coating technique over the anode current collector, followed by a heat treatment at 900 ºC for 1 h in air. Figure 1 shows the schematic diagram of the electrolyte-supported single cell fabricated.

The single cell was set up in a three-atmosphere test bench comprised of two alumina tubes (anode and cathode side) using gold ring and glass for sealing. After sealing treatment and the anode's reduction, the cell was characterized under H_2/He mixture fuel at 800 ºC. The EOCM tests were conducted at 800 ºC and under different reactional conditions, such as CH_4 concentration and the applied current. The anode outlet was heated at 80 ºC along all tests and it was connected to an online gas analyzer setup (GC/MSD). Calibration of the GC/MS system was performed by using commercial standard mixtures of the reactants and products. All electrochemical measurements were performed with a Solartron 1250 potentiostat.

As the reaction is controlled by the electrochemically pumped oxygen ions through the electrolyte, the O^{2-} transfer flux (J) of from the cathode to the anode and the current (I) is given by the Faraday law (Equation 7), then it is possible to calculate the total amount of O_2 feed for the EOCM tests.

$$J\ (mol.s^{-1}) = I \div (2 \times F) \quad [7]$$

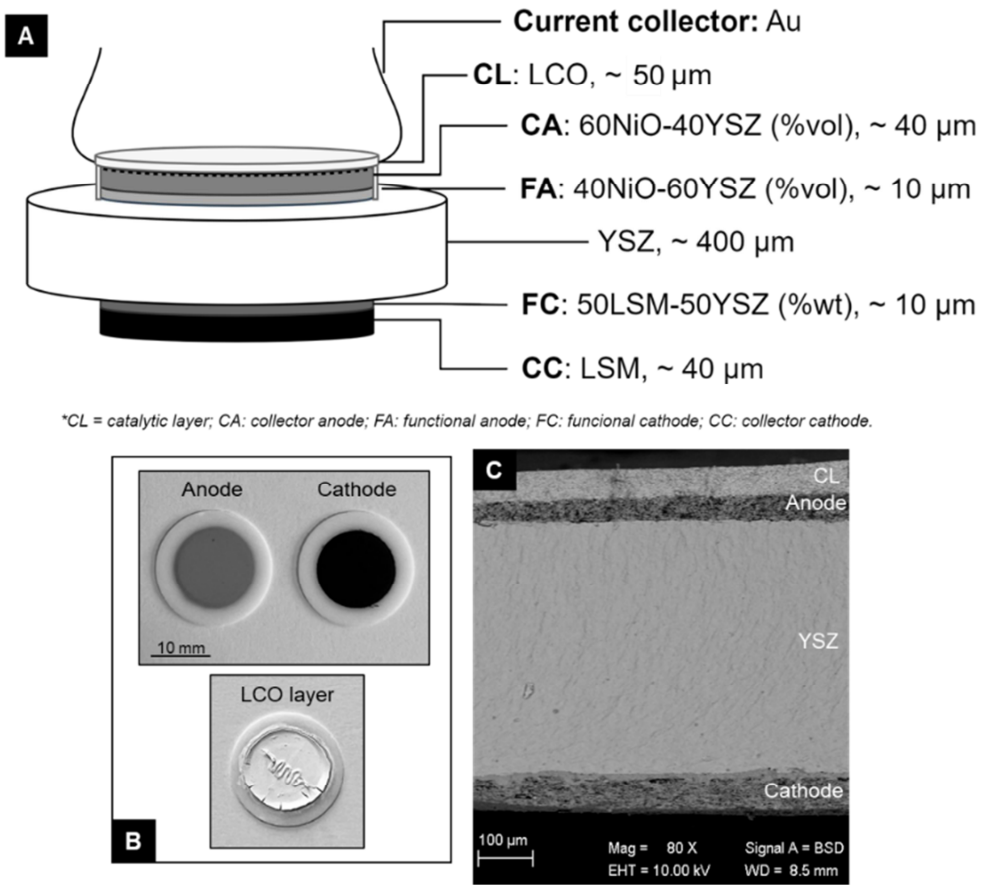

Figure 1. (a) Schematic configuration of the fabricated fuel cell components composition and thickness. (b) Fuel cell electrodes before and after catalytic layer deposition. (c) SEM image of the cross section of the sample after the EOCM test.

Results and Discussion

The XRD patterns in Figure 2a showed that LCO solid solution has a disordered fluorite crystalline structure. The Raman spectra (Fig. 2b) revealed four bands: the A_{1g} band, at 255 cm^{-1}, associates with the formation of lattice oxygen vacancies, the F_{2g} band at 448 cm^{-1} is attributed to the vibrational mode of fluorite structure, the 571 cm^{-1} band refers to the surface oxygen vacancies generated by the random distribution of La^{3+} and Ce^{4+} in the cell, and a band related to surface oxygen vacancies is shown at 1198 cm^{-1}. The formation of surface oxygen vacancies may benefit the OCM reaction, due to such specie acting as active sites, contributing to a more effective catalyst (11,12). SEM images (Fig. 2c) evidenced a microstructure composed of porous agglomerated particles, expected from the combustion synthesis.

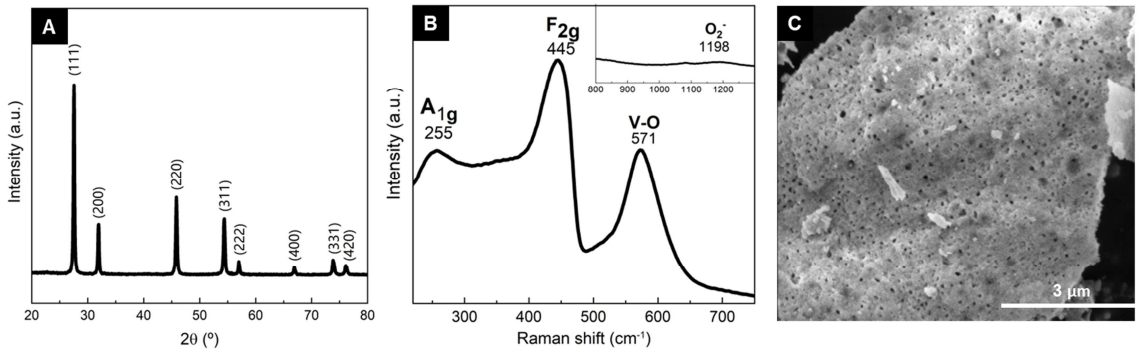

Figure 2. (a) XRD pattern, (b) Raman spectra and (c) SEM image of LCO obtained by combustion method.

CeO_2 is active for the conversion of CH_4, but has little selectivity for OCM, due to its low ability to form electrophilic oxygen species. The interaction of oxides based on rare earth metals was exploited to improve C_2 selectivity. Thus, highlighting $La_{0.5}Ce_{0.5}O_{1.75}$, since La_2O_3 is considered one of the most active and selective materials among earth metal oxides rare due to their high basicity. The existence of the disordered defective cubic phase in the $La_{0.5}Ce_{0.5}O_{1.75}$.catalyst causes an ideal interaction between the surface electrophilic oxygen and the alkaline sites, favoring the C_2 selectivity in the OCM (13).

LCO was active to produce C_2 hydrocarbons, as shown in Figure 3, however, it showed a higher production of CO_x. The LCO selectively produces more C_2H_4, as wanted. Furthermore, physicochemical characterizations of this post-reaction catalyst showed that there was no coke formation, and the catalyst maintained its crystalline structure even after 20 h of reaction.

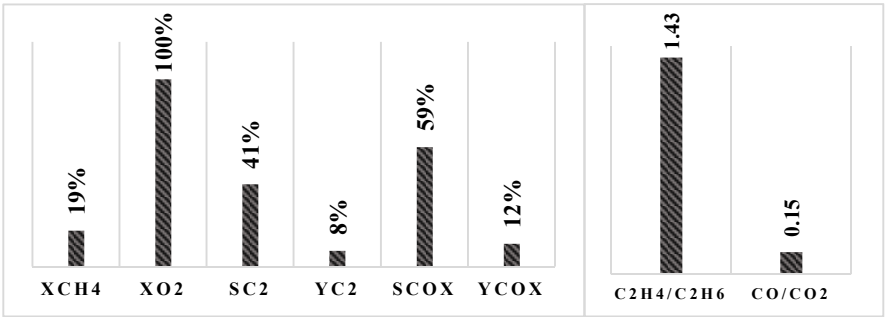

Figure 3. The activity of LCO in the OCM reaction. Reaction conditions: 20 mg of catalyst, 60 mL.min^{-1} gas feed, $4CH_4$:$1O_2$, 800 ^oC, 20 h. *X = conversion, S = selectivity, and Y = yield.

The electrochemical characterization of the prepared fuel cell was developed under an anode flow of 50 mL.min^{-1} H_2/He (10/90%) and a synthetic air flow of 90 ml.min^{-1} on the cathode side, at 800 ºC. The impedance spectra and the polarization curve obtained at 800 ºC are shown in Figure 4. The achieved open-circuit voltage (OCV) was 1.01 V, indicating that the system was gas tightened. The highest maximum power density of 100 mW·cm^{-2} was obtained. The I-V curve (Fig. 4a) shows a linear behavior, suggesting that ohmic losses are dominating over the performance of the fuel cell.

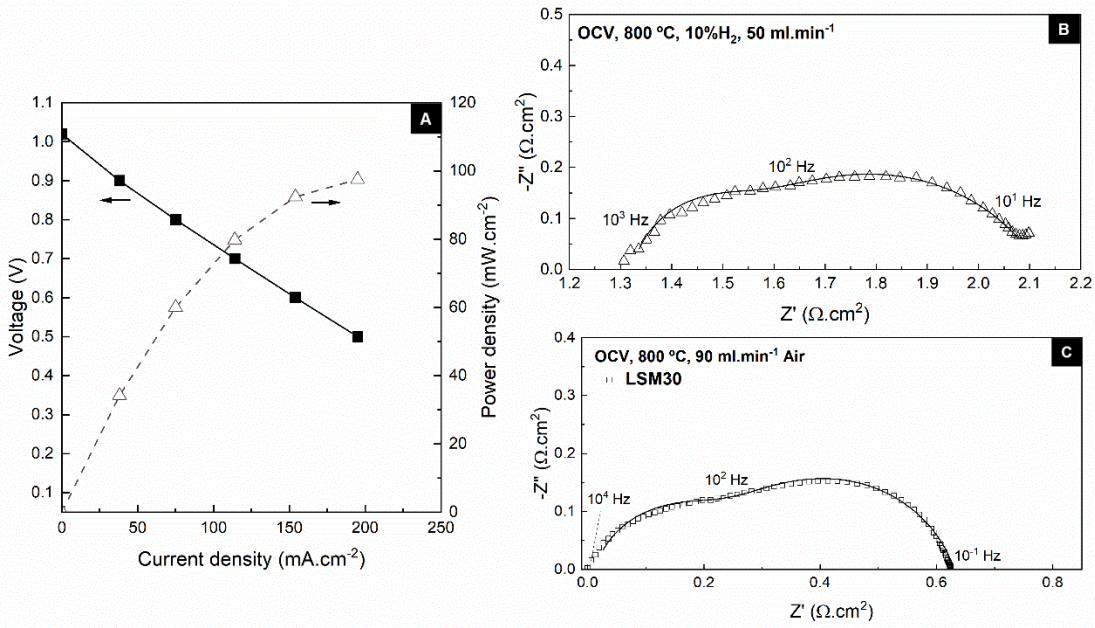

Figure 4. Fuel cell characterization under hydrogen feeding at 800 ºC: (a) Current-voltage (I-V) and current-polarization (I-P) curves, (b) EIS diagrams in OCV obtained after polarization. (c) EIS diagram of an LSM | YSZ | LSM symmetrical cell obtained at 800 ºC (The ohmic resistance was subtracted from the EIS diagram).

The series resistance (R_s) of the cell is attributed to the ohmic resistance and to current collection. The polarization resistance (R_{pol}) is attributed to charge transfer mechanisms, mass diffusion, and reactions occurring at the electrodes. The serial and polarization resistances obtained through the fitting for the fuel cell were 1.3 and 0.78 $\Omega.cm^2$, respectively. And for the LSM symmetrical cell, 1.8 and 0.65 $\Omega.cm^2$. In this case, the cathodic process might lead the R_{pol}, as it could be observed by comparing the resistances obtained of the fuel cell (Fig. 4b) to the LSM symmetrical cell (Fig. 4c). Taking a closer look, in the EIS diagram of the fuel cell, it is possible to observe the presence of an additional component in lower frequency range, which could be related to the catalytic layer contribution, and its diffusion processes. This contribution at lower frequency does not have a considerably contribution on the total resistance (R_{tot}) of the cell. The value of R_{tot} calculated using the I-V curve data is R_{tot} = 2.3 $\Omega.cm^2$, close to the R_{tot} measured by the EIS fitting.

The methane conversion, C_2 selectivity, and yield are closely related to the O^{2-}/CH_4 ratio, which in turn is determined by the current applied and methane feeding rate. For the EOCM tests developed, the values of current applied and amount of CH_4 were chosen to reach the O^{2-}/CH_4 ratio lower than 1, favouring the partial oxidation of methane (14). The total flow at the anode side was maintained constant (50 $mL.min^{-1}$) for the different O^{2-}/CH_4 ratio. To reach O^{2-}/CH_4 = 0.06 ratio, it was applied 40 mA and 10 % of CH_4 of the total flow. For the O^{2-}/CH_4 ratios 0.12 and 0.30, it was applied 40 mA and 5 % of CH_4, and 100 mA and 5 % of CH_4, respectively. For each condition, the result obtained by the online GC/MS gas-analysis of the anode outlet is shown in Table 1.

O^{2-}/CH_4	XCH_4	SC_2	YC_2	SCO_x	YCO_x	SH_2	YH_2	C_2H_4/C_2H_6	CO/CO_2
0.06	65%	3%	2%	8%	5%	81%	54%	0.7	0.18
0.12	67%	7%	5%	16%	10%	74%	60%	0.9	0.03
0.30	68%	4%	3%	23%	16%	70%	63%	0.7	0.04

Table 1. Summary of the EOCM performance of the cell CH_4/LCO/Ni-YSZ│YSZ│LSM/Air, anode total flow 50 mL.min^{-1} at 800 ºC. Anode area 1.2 cm^2.

In this study, oxygen was found to be converted at a high rate (> 95 %) under all experimental conditions. This reduces the likelihood of explosive gas mixture formation of methane and oxygen in the anode compartment.

The CH_4 conversion increased slightly when increasing the O^{2-}/CH_4 ratio in the investigated range. The C_2 selectivity and yield exhibited a maximum (7 %) at O^{2-}/CH_4 = 0.12, while the yield of carbon oxides (CO + CO_2) increased with increasing O^{2-}/CH_4 (15,16). At the lowest applied current (O^{2-}/CH_4 = 0.06), the high H_2 and CO selectivity indicate that the methane reforming reaction was favored (17,18).

There are two pathways for the formation of ethylene: gas-phase dehydrogenation of ethane and a surface route that involves oxygen anion lattice sites on the catalyst (15). The production of ethylene compared to ethane was observed to be favored under experimental conditions that reached the O^{2-}/CH_4 = 0.12. This behavior is possibly attributed to both the quantity and the variety of active oxygen species necessary for CH_4 activation and the conversion of C_2H_6 to C_2H_4 in the catalytic layer surface.

The experimental results showed the successful operation of a fuel cell system for the oxidative coupling of methane and electricity cogeneration, using LCO as a catalyst. The obtained electrochemical data showed good stability indicating resistance to coke, as inferred from the lack of evident coke formation after EOCM tests carried out for more than six hours. However, further investigations are required to stabilize and enhance the catalytic activity in this fuel cell configuration. Microstructural optimization, such as increased porosity and reducing the thickness of the catalytic layer, can enhance both the gas diffusion and the active surface area for the reaction that are likely to improve the performance.

The correlation between CH_4 conversion and C_2 selectivity is closely related to the operating conditions such as temperature, flow rate and concentration of CH_4 feed at the anode, and oxygen concentrations/applied current. Further research should be carried out to identify the ideal operating conditions for EOCM. The use of SOFC as an OCM system is appealing due to the possibility of generating electricity as a by-product. However, the presence of oxygen-containing species leads to the oxidation of CH_4 into CO and CO_2, posing a challenge for both SOFC and SOEC.

Conclusion

The combined results of solid oxide fuel cell and fixed bed reactor showed that the LCO is an active material to the OCM. For the EOCM process, it was shown that the

selectivity of C_2 products is dependent on the O^{2-}/CH_4 ratio, in which higher oxygen content favors the formation of complete oxidation products. Further optimization is necessary to achieve a more efficient system for EOCM. However, the utilization of SOFC for the EOCM with a catalytic layer showed good stability to coke formation and electricity generation as a by-product.

Acknowledgments

This work has been supported by the Center of Innovation on New Energies (CINE), São Paulo Research Foundation (FAPESP), Federal University of ABC (UFABC), and Nuclear and Energy Research Institute (IPEN-CNEN). We are thankful for the funding from CINE Shell / ANP - FAPESP (2017/11937-4) support. F.C.F., A.S.F., and D.Z.F. are fellows of the Brazilian CNPq.

References

1. V. V. Thyssen, V. B. Vilela, D. Z. De Florio, A. S. Ferlauto, and F. C. Fonseca, *Chem Rev* **122**(3), 3966–3995 (2022).
2. T. M. Gür, *Prog Energy Combust Sci* **54**, 1–64 (2016).
3. K. Otsuka Katsuo Suga, and I. Yamanaka, *Catalysis Today* **6**, 587–592 (1990).
4. W. Deibert, M. E. Ivanova, S. Baumann, O. Guillon, and W. A. Meulenberg, *J Memb Sci* **543**, 79–97 (2017).
5. E. Perry Murray, T. Tsai, and S. A. Barnett, *Nature* **400**(6745), 649–651 (1999).
6. T. Kawada, M. Sase, M. Kudo, K. Yashiro, K. Sato, J. Mizusaki, N. Sakai, T. Horita, K. Yamaji, and H. Yokokawa, *Solid State Ion* **177**(35–36), 3081–3086 (2006).
7. N. U. Pujare and A. F. Sammells, *J Electrochem Soc* **135**(10), 2544–2545 (1988).
8. K. Liu, J. Zhao, D. Zhu, F. Meng, F. Kong, and Y. Tang, *Catal Commun* **96**, 23–27 (2017).
9. C. Zhu, S. Hou, X. Hu, J. Lu, F. Chen, and K. Xie, *Nature Communications* **10**(1), 1–8 (2019).
10. V. B. Vilela, V. V. Thyssen, L. N. Rodrigues, and F. C. Fonseca, *ECS Trans* **103**(1), 1917–1925 (2021).
11. J. Zamudio-García, J. Porras-Vázquez, J. Canales-Vázquez, A. Cabeza, L. Losilla, and D. Marrero-López, *Inorg Chem* **58**(14), 9368–9377 (2019).
12. Y. Zhang, J. Xu, X. Xu, R. Xi,Y. Liu, X. Fang, and X. Wang, *Catal Today* **355**(April), 518–528 (2020).
13. C. A. Ortiz-Bravo, C. A. Chagas, and F. S. Toniolo, *J Nat Gas Sci Eng* **96** (2021).
14. Z. Zhan, Y. Lin, M. Pillai, I. Kim, and S. A. Barnett, *J Power Sources* **161**(1), 460–465 (2006).
15. D. J. Kuchynka, R. L. Cook, and A. F. Sammells, *J Electrochem Soc* **138**(5), 1284–1299 (1991).
16. T. J. Mazanec, T. L. Cable, and J. G. Frye, *Solid State Ion* **53–56**, 111–118 (1992).
17. S. A. Venâncio, B. J. M. Sarruf, G. G. Gomes, and P. E. V. de Miranda, *Int J Hydrogen Energy* **45**(8), 5501–5511 (2020).
18. O. A. Marina and M. Mogensen, *Appl Catal A Gen* **189**(1), 117–126 (1999).